Ordering due to Quantum Fluctuations in $Sr_2Cu_3O_4Cl_2$

Y. J. Kim,[1,2] A. Aharony,[3] R. J. Birgeneau,[1] F. C. Chou,[1] O. Entin-Wohlman,[3] R. W. Erwin,[4] M. Greven,[1,*] A. B. Harris,[5] M. A. Kastner,[1] I. Ya. Korenblit,[3] Y. S. Lee,[1] and G. Shirane[6]

[1]*Center for Materials Science and Engineering, Massachusetts Institute of Technology, Cambridge, Massachusetts 02139*
[2]*Division of Engineering and Applied Sciences, Harvard University, Cambridge, Massachusetts 02138*
[3]*School of Physics and Astronomy, Tel Aviv University, Tel Aviv 69978, Israel*
[4]*National Institute of Standards and Technology, Gaithersburg, Maryland 20899*
[5]*Department of Physics, University of Pennsylvania, Philadelphia, Pennsylvania 19104*
[6]*Department of Physics, Brookhaven National Laboratory, Upton, New York 11973*

(Received 4 January 1999)

$Sr_2Cu_3O_4Cl_2$ has Cu_I and Cu_{II} subsystems, forming interpenetrating $S = 1/2$ square lattice Heisenberg antiferromagnets. The classical ground state is degenerate, due to frustration of the intersubsystem interactions. Magnetic neutron scattering experiments show that quantum fluctuations cause a two dimensional Ising ordering of the Cu_{II}'s, lifting the degeneracy, and a dramatic increase of the Cu_I out-of-plane spin-wave gap, unique for *order out of disorder*. The spin-wave energies are quantitatively predicted by calculations which include quantum fluctuations.

PACS numbers: 75.30.Ds, 75.10.Jm, 75.25.+z, 75.45.+j

The classical ground states of many magnetic systems are degenerate due to frustration. Quantum or thermal fluctuations often lift this degeneracy, yielding *order due to disorder* [1–4]. For example, when a system can be separated into two Heisenberg antiferromagnetic (AFM) sublattices, so that the molecular field of the spins in each sublattice vanishes on the spins of the other, then classically the sublattices order independently of each other, the ground state is degenerate, and the excitation spectrum contains two distinct sets of zero energy (Goldstone) modes, reflecting the fact that these subsystems can be rotated independently without cost in energy. As shown by Shender, quantum spin-wave (SW) interactions prefer collinearity of the spins in the two sublattices [2]. Concomitantly, this also generates a *fluctuation driven gap* in the SW spectrum. Indeed, such a gap was hypothesized in the garnet $Fe_2Ca_3(GeO_4)_3$ [5]. Since a similar gap could also arise from crystalline magnetic anisotropy, the final identification was rather complex.

In parallel to these developments, the discovery of high temperature superconductivity triggered much work on the magnetism in lamellar copper oxides. These materials contain CuO_2 planes, whose two-dimensional (2D) spin fluctuations can be modeled well by the $S = 1/2$ square lattice quantum Heisenberg antiferromagnet (SLQHA) [6].

The above two advances combine in the isostructural compounds $Sr_2Cu_3O_4Cl_2$ and $Ba_2Cu_3O_4Cl_2$ (2342). In the present paper, we show that these materials offer a dramatic and clear demonstration of ordering due to fluctuations. As shown in Fig. 1(a), the CuO_2 plane is replaced in 2342 by a Cu_3O_4 one, which contains an additional Cu_{II}^{2+} ion at the center of every second plaquette of the original Cu_IO_2 square lattice [7]. The configuration in the neighboring plane is obtained by translating the whole plane by $(\frac{a}{2}\ \frac{a}{2})$. In the plane, the Cu_I and Cu_{II} subsystems form interpenetrating $S = 1/2$ SLQHA's with exchange interactions J_I and J_{II}. The isotropic interaction $J_{I\text{-}II}$ between these subsystems is frustrated; that is, its molecular field vanishes as described above, and one needs nontrivial theories to explain their ordering and SW gaps. Experimentally, 2342 exhibits AFM order of the Cu_I's and Cu_{II}'s below the Néel temperatures $T_{N,I}$ and $T_{N,II}$, respectively [8,9]. For temperatures $T > T_{N,II}$, the Cu_{II} susceptibility behaves as in a SLQHA, with $J_{II} \sim 10$ meV [10]. $J_I \sim 130$ meV is known from other cuprates. For $T < T_{N,II}$, the magnetization data were interpreted assuming Shender collinearity [10].

This paper reports on theory and neutron scattering experiments in $Sr_2Cu_3O_4Cl_2$. The inelastic neutron data show a dramatic increase of the Cu_I "out-of-plane" [11]

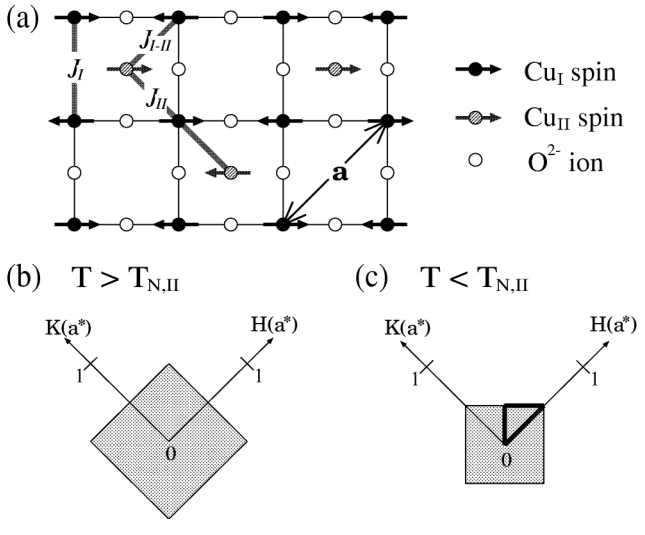

FIG. 1. (a) Magnetic structure of the Cu_3O_4 plane in 2342 at $T < T_{N,II}$. The corresponding 2D reciprocal lattices are shown in (b) for $T > T_{N,II}$, and in (c) for $T < T_{N,II}$. The shaded area is the 2D Brillouin zone.

 0031-9007/99/83(4)/852(4)$15.00

gap below $T_{N,\mathrm{II}}$ (see Fig. 2), which clearly reflects a coupling between the Cu_I and Cu_{II} spins. However, since symmetry indicates that within mean field theory this coupling due to frustrated interactions must vanish, we conclude that the enhanced gap for $T < T_{N,\mathrm{II}}$ is *due to fluctuations*. This identification is particularly strong, since our data are quantitatively predicted by detailed theoretical calculations, which use parameters determined independently, albeit less accurately, by the static measurements [10]. The SW dispersion along (1 0 L), shown in Fig. 3, depends crucially on the fluctuations. In contrast, most of the in-plane dispersion is described by the linear SW theory. A nontrivial exception arises near the zone boundary of the Cu_{II}'s, which we could access with thermal neutrons because of the small J_{II}. Figure 4 exhibits a novel dispersion, which is shown to result from the quantum nature of the SLQHA.

Since the SLQHA does not have long-range order at $T > 0$, such order must arise from spin anisotropy terms or interplane couplings. Our data indicate that $T_{N,\mathrm{I}} \sim 385$ K is determined by the latter, via $\xi_0(T_{N,\mathrm{I}})^2 J_{\mathrm{I,3D}}/J_{\mathrm{I}} \sim 1$, with $J_{\mathrm{I,3D}} \sim 0.1$ meV. Here, $\xi_0(T)$ is the SLQHA correlation length [6,12]. The spin structure, shown in Fig. 1(a), has been uniquely determined from analyzing 13 different neutron diffraction peaks in the plane [13], confirming the conjecture in Ref. [10]. As in $YBa_2Cu_3O_6$ [14], the Cu_I spins order along the Cu_I-Cu_{II} bonds, as expected when the quantum fourfold anisotropy is dominant [15]. Unlike the Cu_I's, the interplane Cu_{II}-Cu_{II} coupling is frustrated, similar to that in $Sr_2CuO_2Cl_2$ [6], and therefore $T_{N,\mathrm{II}}$ is expected to be determined mainly by in-plane spin anisotropies. Indeed, the 2D nature of the Cu_{II} subsystem has been established from both the existence of rods of 2D scattering for $T > T_{N,\mathrm{II}}$ and the small SW dispersion along L [13]. For $T < T_{N,\mathrm{I}}$, the ordered Cu_I spins fluctuate mainly in the directions transverse to their staggered moment $\mathbf{M}_{s,\mathrm{I}}$. $J_{\mathrm{I\text{-}II}}$ then generates fluctuations in the Cu_{II} spins along the same directions, causing an effective reduction in the corresponding transverse exchange components of J_{II} [2]. This yields an effective term $-\tilde{\delta}(\mathbf{M}_{s,\mathrm{I}} \cdot \mathbf{S}_{\mathrm{II}})^2$, where $\tilde{\delta} \propto J_{\mathrm{I\text{-}II}}^2/(J_{\mathrm{I}} + J_{\mathrm{II}})$. This implies an Ising-like anisotropy $J_{\mathrm{II}}\alpha_{\mathrm{II}}^{\mathrm{eff}} \propto \tilde{\delta}\mathbf{M}_{s,\mathrm{I}}^2$, which favors ordering of the Cu_{II} spins collinearly with $\mathbf{M}_{s,\mathrm{I}}$, consistent with our measured structure, Fig. 1(a). Indeed, $T_{N,\mathrm{II}} \sim 40$ K agrees with $\xi_0(T_{N,\mathrm{II}})^2\alpha_{\mathrm{II}}^{\mathrm{eff}} \sim 1$, where $\alpha_{\mathrm{II}}^{\mathrm{eff}} \sim 0.01$ was deduced from our SW gaps. Heuristically, the lowering of the symmetry on the Cu_{II} site due to the ordering of the Cu_I's is sensed through the quantum fluctuations.

Large ($\sim$2 cm^3) single crystals of $Sr_2Cu_3O_4Cl_2$, grown by slow cooling of a melt containing CuO flux, are used in the experiment. The crystal remains tetragonal for $15 < T < 550$ K [10]. Our neutron scattering experiments were carried out with the triple-axis spectrometers at the High Flux Beam Reactor, Brookhaven National Laboratory, and at the National Institute of Standards and Technology Research Reactor. Collimation of 40′-40′-S-40′-80′ and fixed final neutron energy of 14.7 meV were used for most of the inelastic measurements. When better resolution was required, we used a fixed initial neutron energy of 13.7 meV and tighter collimations.

The T dependences of $M_{s,\mathrm{I}}$ and $M_{s,\mathrm{II}}$ [proportional to the square root of the AFM Bragg intensities at the (1 0 1) and the ($\frac{1}{2}$ $\frac{1}{2}$ 0) reciprocal positions, respectively] are shown in Fig. 2(a). Since nuclear Bragg scattering is only weakly T dependent, we subtract the high-temperature (1 0 1) nuclear intensity from the observed intensity. The solid lines in Fig. 2(a) represent $M_s \sim (T_N - T)^{\beta}$. The parameters given there were fitted for

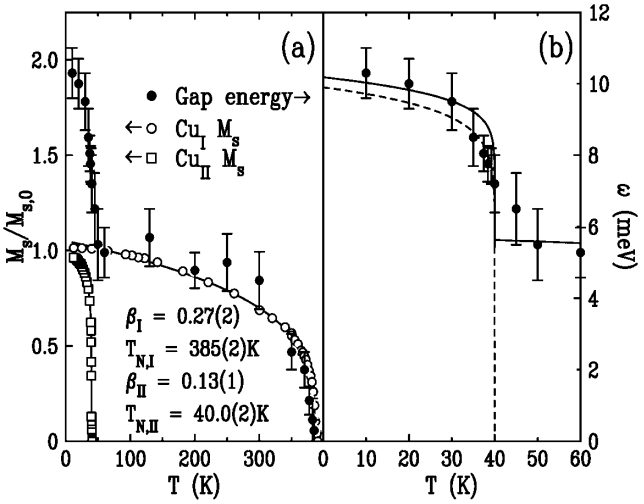

FIG. 2. (a) Temperature dependence of the Cu_I out-of-plane gap energy and of the staggered magnetizations M_s of Cu_I and Cu_{II}. M_s is normalized to the extrapolated zero temperature value $M_{s,0}$. The solid lines are the results of fits to the form $\sim(T_N - T)^{\beta}$. (b) The gap energy in a different temperature scale. The solid and dashed lines are interpolations for ω_4 and ω_3; see text.

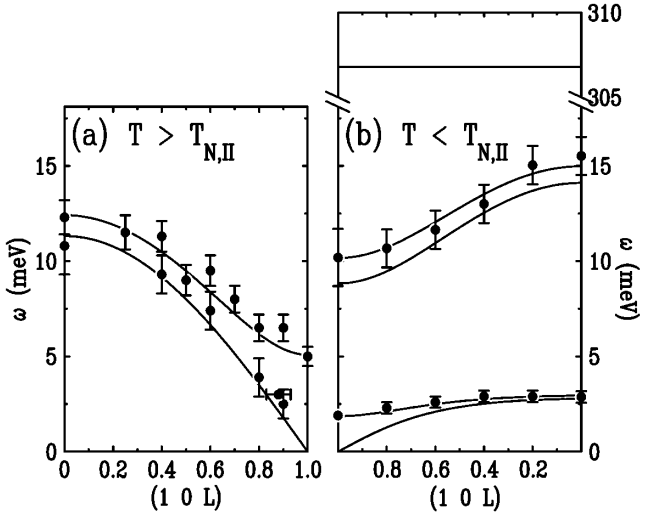

FIG. 3. (a) Magnon dispersion along the L direction at the 2D zone center for $T = 200$ K (solid circles). (b) Same for $T = 10$ K. The solid lines show Eq. (2).

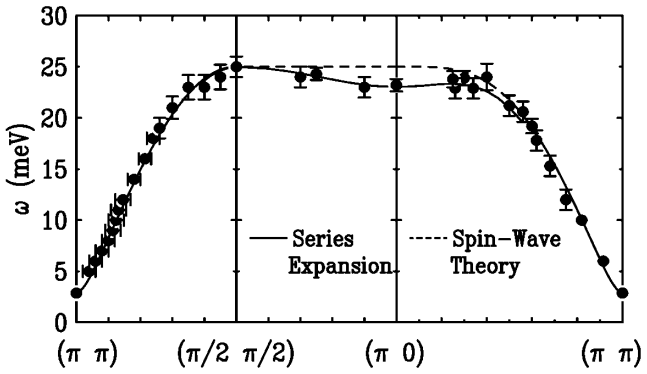

FIG. 4. Cu_{II} in-plane SW dispersion at $T = 10$ K.

$T > 200$ K (Cu_I) and $T > 25$ K (Cu_{II}). $\beta_{II} = 0.13(1)$ clearly demonstrates the 2D Ising criticality of the Cu_{II} ordering. $T_{N,I} = 385(2)$ K and $T_{N,II} = 40.0(2)$ K agree with those from our previous magnetization study [10], while $\beta_I = 0.27(2)$ is consistent with that of $Sr_2CuO_2Cl_2$ and La_2CuO_4 [6].

Our measured SW energies are all explained within a $T = 0$ interacting SW theory. We start from the "minimal" Hamiltonian

$$\mathcal{H} = \sum_{\langle i,j\rangle_I} \sum_{\mu} J_I^{\mu} S_i^{\mu} S_j^{\mu} + J_{I,3D} \sum_{\langle i,j\rangle_{I,3D}} \mathbf{S}_i \cdot \mathbf{S}_j + \sum_{\langle m,n\rangle_{II}} \sum_{\mu} J_{II}^{\mu} S_m^{\mu} S_n^{\mu} + J_{I\text{-}II} \sum_{\langle i,m\rangle_{I\text{-}II}} \mathbf{S}_i \cdot \mathbf{S}_m , \quad (1)$$

where i, j and m, n denote Cu_I sites and Cu_{II} sites, respectively, and where we assume that $J_A^a = J_A^b = J_A$ and $J_A^c = J_A(1 - \alpha_A)$ for $A = I, II$ and $\mu = a, b, c$. We also assume that $J_I \gg J_{II}, J_{I\text{-}II}$. The effects of other (smaller) terms, such as the various in-plane anisotropies [10,15], will be presented elsewhere [16]. $\langle i,j\rangle_I$ and $\langle i,j\rangle_{I,3D}$ label Cu_I intra- and interplanar nearest neighbors (NN's), whereas $\langle m,n\rangle_{II}$ and $\langle i,m\rangle_{I\text{-}II}$ refer to the NN Cu_{II}-Cu_{II} and Cu_I-Cu_{II} bonds, respectively. Starting from the spin structure shown in Fig. 1(a), we express each of the six spins in the unit cell by the Holstein-Primakoff transformation for general spin S. The first three sums in $\mathcal{H}$ are then truncated at the harmonic order in the SW boson operators. However, the $J_{I\text{-}II}$ term vanishes at the zone center, and therefore has effects only if one expands it to quartic order. We then approximate each product of four SW operators by contracting operator pairs in all possible ways. This yields new quadratic terms, whose coefficients contain the parameter $\delta = 2J_{I\text{-}II}\langle ae\rangle/S \propto \tilde{\delta}$, where a and e are boson operators associated with Cu_I and Cu_{II}, respectively. This coefficient contains the factor $1/S$, thus representing quantum corrections due to SW interactions. The SW energies are then found as the eigenvalues of the 6×6 matrix which arises from the resulting bilinear SW Hamiltonian [16].

The resulting $T = 0$ magnon modes can be found analytically along the L direction at the 2D zone center [(1 0 L) reciprocal lattice points, $q_c \equiv 2\pi L/c$]. In addition to the two optical modes, which are practically degenerate at $\omega \approx 4SZ_cJ_I$, the low-energy modes are (in order of increasing energy)

$$\omega_1 = S\sqrt{32J_{II}\delta x_3/(\delta + 2x_3)}, \quad (2a)$$

$$\omega_2 = S\sqrt{32J_{II}\left(Z_g^2 J_{II}\alpha_{II} + \frac{\delta(2J_I\alpha_I Z_g^2 + x_3)}{4J_I\alpha_I Z_g^2 + \delta + 2x_3}\right)}, \quad (2b)$$

$$\omega_3 = S\sqrt{8J_I(\delta + 2x_3)}, \quad (2c)$$

$$\omega_4 = S\sqrt{8J_I(4Z_g^2 J_I\alpha_I + \delta + 2x_3)}, \quad (2d)$$

where $Z_c = 1 + O(1/S) \approx 1.17$ [17] and $Z_g = 1 + O(1/S) \approx 0.6$ [18] are the quantum renormalization factors for the SW velocity and for the SW anisotropy gap when $S = 1/2$, and $x_3 = Z_3^2 J_{I,3D}[1 + \cos(\pi L)]$, where $Z_3 = 1 + O(1/S) \approx 0.9$ [16]. In Eq. (2) we keep only terms up to $O(1/S)$ [which leaves some ambiguity in the ratios appearing in Eqs. (2a) and (2b)]. Since $\delta = O(1/S)$, this term is not renormalized. Note that the dispersion of ω_1 and ω_2 is of order δ, and hence is purely fluctuational.

Figure 3 shows our measured dispersion along the L direction, together with fits to Eq. (2), above and below $T_{N,II}$. The momentum transfer is held constant at (1 0 L), and the energy transfer is varied at each T. For $T > T_{N,II}$, our theory predicts only two acoustic modes, whose energies are given by ω_3 and ω_4 with $\delta = 0$. Far below $T_{N,I}$, these can be approximated by the low-T results in Eq. (2). Fixing $J_I = 130$ meV and $\delta = 0$, we fit the gapless data to ω_3, and obtain $J_{I,3D} = 0.14(2)$ meV. Identifying the data with the gap with ω_4, that is, with the out-of-plane Cu_I mode, we then fit Eq. (2d) and find $\alpha_I = 5.2(9) \times 10^{-4}$. This value is consistent with that ($\approx 1.5 \times 10^{-4}$) found in $Sr_2CuO_2Cl_2$, if the anisotropy gap is renormalized by Z_g rather than by Z_c (as incorrectly done in Ref. [6]).

Below $T_{N,II}$, Eq. (2) predicts four different low-lying modes. However, as seen in Fig. 3(b), our experiment seems to show only two low-energy modes. We interpret the higher of these as an overlap of ω_4 and ω_3, which could not be resolved due to the resolution and the existence of a nearby phonon peak. We emphasize that for $T < T_{N,II}$, $\omega_3 > 0$ at $L = 1$ is a pure quantum effect; the close values of ω_3 and ω_4 simply reflect the fact that the effective anisotropy associated with δ is larger than the intrinsic Cu_I anisotropy α_I [see Eqs. (2c) and (2d)], thus illustrating the quantitative importance of the *order due to disorder* effects. The lower mode is identified as ω_2. The experimental resolution did not permit identifying ω_1 as a distinct mode. The solid lines in Fig. 3(b) were drawn using Eq. (2), with $\delta = 0.3(1)$ meV, $J_{II} = 10.5$ meV (see below and Ref. [10]) and $\alpha_{II} = 0.0001(5)$. We found δ by fitting ω_3 and ω_4 with fixed J_I, and α_{II} by then fitting ω_2 with fixed $J_{II} = 10.5$ meV. The error bar allows $\alpha_{II} = 0$.

Given the uncertainties, the theory agrees well with the data. Our measured value of $\delta \propto \tilde{\delta}$ is consistent with $|J_{\text{I-II}}| \sim 10$ meV, as found in our earlier magnetization study [10]. Both the ω_1 and ω_2 modes at $L = 1$ have been observed with microwave resonance techniques in $Ba_2Cu_3O_4Cl_2$ [8], but not yet in $Sr_2Cu_3O_4Cl_2$. The $Ba_2Cu_3O_4Cl_2$ results are consistent with Fig. 3(b).

Figure 2 shows the T dependence of ω_4 at the zone center, $L = 1$. In agreement with Eq. (2d), the appearance of a nonzero δ causes a unique and dramatic increase in this gap. Similar to tetragonal SLQHA's K_2NiF_4 ($S = 1$) [19] and $Sr_2CuO_2Cl_2$ ($S = 1/2$) [6], this out-of-plane gap roughly follows $M_{s,\text{I}}$ for $T > T_{N,\text{II}}$ [see Fig. 2(a)]. Below $T_{N,\text{II}}$, the measured gap represents both ω_3 and ω_4. The full and dashed lines in Fig. 3(b) represent Eqs. (2d) and (2c), respectively, in which we multiplied δ by $(M_{s,\text{II}}/M_{s,\text{II},0})^2$ (as in our estimate for $\alpha_{\text{II}}^{\text{eff}}$), to interpolate between 0 K and the low-T value.

In addition to the above results, we also measured SW's in the ab plane, along the high-symmetry directions shown as thick lines in Fig. 1(c). Here, $(\pi\ \pi)$ is the $(\frac{1}{2}\ \frac{1}{2}\ 0)$ magnetic Bragg peak position. However, because there are two types of AFM domains due to the tetragonal structure, we are actually measuring contributions from both the $(\frac{1}{2}\ \frac{1}{2}\ 0)$ and the $(\frac{1}{2}\ \bar{\frac{1}{2}}\ 0)$ positions. Figure 4 summarizes our results at 10 K, which is well below $T_{N,\text{II}}$. Both constant energy-transfer scans and constant momentum-transfer scans were carried out. From the zone boundary SW energy of 25 meV one can deduce J_{II} rather accurately as $J_{\text{II}} = 10.5(5)$ meV, in excellent agreement with the value deduced before from the Cu_{II} susceptibility [10]. The gap energy at the zone center, ~ 3 meV, corresponds to the lower gap found at $L = 0$ in Fig. 3(b). It turns out that ω_3 and ω_4 are not observed at the $(\frac{1}{2}\ \frac{1}{2}\ 0)$ position, due to small intensity.

Away from the 2D zone center, ω_1 and ω_2 are degenerate and can be approximated as a simple SLQHA with the exchange J_{II}. With $\alpha_{\text{II}} \approx 0$, Eq. (2b) can be interpreted as resulting from an effective anisotropy given by $J_{\text{II}}\alpha_{\text{II}}^{\text{eff}} = 2J_{\text{I}}\alpha_{\text{I}}\delta/(4J_{\text{I}}\alpha_{\text{I}} + \delta) \approx 0.1$ meV, or $\alpha_{\text{II}}^{\text{eff}} \approx 0.01$. Using the simple (large S) harmonic approximation described above with this value and $J_{\text{II}} = 10.5$ meV gives the dashed line in Fig. 4. This is a good approximation, except for the dispersion near the zone edge $(\pi\ 0)$. As seen by the continuous line, our data are in much better agreement with recent series expansion results by Singh and Gelfand [20], calculated with the same parameters. This theory predicts a local minimum at $(\pi\ 0)$, lower by about 7% than the value at $(\frac{\pi}{2}\ \frac{\pi}{2})$. This dispersion is a pure quantum mechanical effect for the $S = 1/2$ NN Heisenberg model. A nonzero dispersion along the zone boundary may also result from a nonzero next-NN (NNN) interaction $J_{\text{II}}^{\text{NNN}}$, within linear SW theory. The magnitude of the dispersion between $(\pi\ 0)$ and $(\frac{\pi}{2}\ \frac{\pi}{2})$ is given by $2SJ_{\text{II}}^{\text{NNN}}$. Considering that J_{II} is already the order of 10 meV and the NNN distance is large (~ 7.7 Å), it is unlikely that the NNN effects contribute strongly to the observed zone-boundary energy difference of ~ 2 meV in $Sr_2Cu_3O_4Cl_2$.

In conclusion, we have shown that quantum fluctuations in $Sr_2Cu_3O_4Cl_2$ lift the classical degeneracy due to the frustration and make Cu_{II} spins order with Ising criticality. We have also shown that the zero-energy modes acquire energy gaps due to the quantum fluctuations, which can be explained quantitatively by the SW calculation including the SW interaction terms.

This work was supported by the U.S.-Israel Binational Science Foundation (at Tel Aviv, MIT, and Penn), by the NSF Grant No. DMR97-04532, and by the MRSEC Program of the NSF under Award No. DMR98-08941 (at MIT), under Contract No. DE-AC02-98CH10886, Division of Material Science, U.S. Department of Energy (at BNL), and by the NSF under agreement No. DMR-9423101 (at NIST).

*Present address: Department of Applied Physics, Stanford University, Stanford, CA 94305.

[1] J. Villain *et al.*, J. Phys. (Paris) **41**, 1263 (1980).
[2] E. F. Shender, Sov. Phys. JETP **56**, 178 (1982).
[3] C. L. Henley, Phys. Rev. Lett. **62**, 2056 (1989); **73**, 2788 (1994).
[4] E. F. Shender and P. C. W. Holdsworth, in *Fluctuations and Order*, edited by M. Milonas (Springer-Verlag, New York, 1995).
[5] A. G. Gukasov *et al.*, Europhys. Lett. **7**, 83 (1988); Th. Brueckel *et al.*, Z. Phys. B **72**, 477 (1988); Phys. Lett. A **162**, 357 (1992).
[6] M. Greven *et al.*, Z. Phys. B **96**, 465 (1995); R. J. Birgeneau *et al.*, J. Phys. Chem. Solids **56**, 1913 (1995).
[7] B. Grande and H. Müller-Buschbaum, Z. Naturforsch. B **31**, 405 (1976); H. Müller-Buschbaum, Angew. Chem., Int. Ed. Engl. **16**, 674 (1977).
[8] N. Adachi *et al.*, Physica (Amsterdam) **201B**, 174 (1994); H. Ohta *et al.*, J. Phys. Soc. Jpn. **64**, 1759 (1995).
[9] K. Yamada *et al.*, Physica (Amsterdam) **213B**, 191 (1995); H. Rosner *et al.*, Phys. Rev. B **57**, 13 660 (1998).
[10] F. C. Chou *et al.*, Phys. Rev. Lett. **78**, 535 (1997); M. A. Kastner *et al.*, Phys. Rev. B **59**, 14 702 (1999).
[11] The term "out-of-plane" denotes the polarization of the SW eigenvector determined from neutron scattering measurements. See, e.g., Ref. [6].
[12] B. Keimer *et al.*, Phys. Rev. B **46**, 14 034 (1992).
[13] Y. J. Kim *et al.* (to be published).
[14] T. Yildirim *et al.*, Phys. Rev. Lett. **72**, 3710 (1994); T. Yildirim *et al.*, Phys. Rev. B **53**, 6455 (1996).
[15] T. Yildirim *et al.*, Phys. Rev. B **52**, 10 239 (1995).
[16] Details will be published elsewhere.
[17] B. B. Beard *et al.*, Phys. Rev. Lett. **80**, 1742 (1998).
[18] We have shown that Z_g for easy-plane anisotropy is the same as that for easy-axis anisotropy, calculated by W. Zheng *et al.*, Phys. Rev. B **43**, 8321 (1991).
[19] R. J. Birgeneau *et al.*, Phys. Rev. B **3**, 1736 (1971).
[20] R. R. P. Singh and M. P. Gelfand, Phys. Rev. B **52**, 15 695 (1995).